scientific reports

Check for updates

OPEN

Arg209Lys and Gln508His missense variants in Rabphilin 3A cause pre- and post-synaptic dysfunctions at excitatory glutamatergic synapses

Marta Barzasi[1], Alessio Spinola[1], Alex Costa[2,3], Lisa Pavinato[4,5], Alfredo Brusco[6,7], Elena Marcello[1], Monica DiLuca[1] & Fabrizio Gardoni[1]✉

The synaptic protein Rabphilin 3A (Rph3A), encoded by the *RPH3A* gene, is a known binding partner of the NMDA receptor (NMDAR) complex, which is essential for synaptic plasticity and cognitive functions. A recent report demonstrated a causal association between missense variants in the *RPH3A* gene and neurodevelopmental disorders, manifesting as either drug-resistant epilepsy with intellectual disability or as autism spectrum disorder with learning disability. In this study, we used primary hippocampal neurons to analyse synaptic effects induced by the p.(Arg209Lys) and p.(Gln508His) *RPH3A* variants, located in the N-terminal disordered region and the C-terminal C2A domain of Rph3A, respectively. We found that both the mutants exert effects on pre- and post-synaptic events mediated by Rph3A, despite their different positions within the Rph3A amino acid sequence. Notably, in both cases, *RPH3A* variants reduced presynaptic glutamate release and led to decreased synaptic retention of NMDARs containing the GluN2A subunit, a primary binding partner of Rph3A. These changes were associated with a reduced frequency of calcium events at dendritic spines, indicating an overall significant dysregulation of glutamatergic synaptic transmission.

Keywords Epilepsy, Excitatory synapse, Neurodevelopmental disorders, Rabphilin 3A, RPH3A

RPH3A encodes the synaptic protein Rabphilin 3A (Rph3A), which is a binding partner of synaptically retained NMDA receptors (NMDARs) at excitatory glutamatergic synapses[1–4]. Rph3A was initially identified as a presynaptic component associated with Rab3A on vesicles[5], and was later shown to be a binding partner of numerous pre- and post-synaptic proteins, including PSD-95[1], CASK[6], synaptotagmin-1[7], SNAP-25[8], Arf6[9], and myosin Va (MyoVa)[10]. We have previously demonstrated that in dendritic spines, Rph3A forms a molecular complex with the GluN2A subunit of NMDARs and the scaffolding protein PSD-95, promoting the synaptic retention of NMDARs[1,2]. Overall, the interaction of Rph3A with the NMDAR complex plays a key role in functional and structural synaptic plasticity, and subsequently in cognitive behaviour[1–3].

Our group described six cases with missense variants in *RPH3A*: p.(Gln73His)dn; p.(Arg209Lys), p.(Arg235Ser), p.(Thr450Ser)dn, p.(Gln508His), and p.(Asn618Ser)dn. These variants present with drug-resistant epilepsy with intellectual disability or as autism spectrum disorder with learning disability[11]. Another report identified variants affecting residues 269 and 464 in an individual with congenital myasthenic syndrome, although the functional and clinical relevance of those changes has not been fully established[12]. Using in vitro cultured hippocampal neurons transfected with mouse ortholog *RPH3A*, we demonstrated that the p.(Thr450Ser) and p.(Asn618Ser) mutations—both located in the C-terminal C2 domains of Rph3A, which are involved in the regulation of activity through calcium/IP_3 binding[7,13]—lead to aberrant activation of NMDARs and alterations in synaptic GluN2A levels[11]. These molecular changes were associated with disrupted cytosolic calcium dynamics at dendritic spines[11].

Considering the numerous synaptic functions of Rph3A and its interactions with various pre- and post-synaptic proteins through its distinct domains, further analyses of the molecular and functional effects of

[1]Department of Pharmacological and Biomolecular Sciences (DiSFeB) "Rodolfo Paoletti", University of Milan, Milan, Italy. [2]Department of Biosciences, University of Milan, Milan 20122, Italy. [3]Institute of Biophysics, Consiglio Nazionale delle Ricerche (CNR), Milan 20133, Italy. [4]Institute of Oncology Research (IOR), BIOS+, Bellinzona 6500, Switzerland. [5]Università della Svizzera Italiana, Lugano 6900, Switzerland. [6]Department of Neurosciences Rita Levi-Montalcini, University of Turin, Turin 10126, Italy. [7]Medical Genetics Unit, Città della Salute e della Scienza University Hospital, Turin 10126, Italy. ✉email: fabrizio.gardoni@unimi.it

additional Rph3A variants are essential to gain a more comprehensive understanding of the pathological roles of disease-associated mutations. Building on the experimental approach from our previous study[11], here we characterised and compared the effects of two variants previously identified in patients[11], p.(Arg209Lys) and p.(Gln508His), located in the disordered N-domain and C2A domain of Rph3A, respectively. Specifically, we took advantage of a mouse hSyn-RFP-Rph3A-WPRE plasmid[3,11] mutagenised in position 206 (corresponding to human 209) or 495 (corresponding to human 508). In particular, we investigated how these variants influence the surface localisation and postsynaptic distribution of GluN2A-containing NMDARs, the CREB-mediated signalling pathway, glutamate release, and calcium dynamics in dendritic spines.

Results

Rph3A missense variants induce impairments of GluN2A-containing NMDAR localisation and availability at the postsynaptic compartment

To understand the relevance of the variants' position among the Rph3A amino acid sequence, we evaluated the putative synaptic modifications induced by two other *RPH3A* missense variants, hRph3A^{R209K} [p.(Arg209Lys)] and hRph3A^{Q508H} [p.(Gln508His)]. The first variant is in a disordered region of Rph3A at the N-terminus; the second is located within the C2A domain but corresponds to a different phenotype compared to the T450S variant located in the same domain. Considering the key role of Rph3A in driving the correct localisation of GluN2A-containing NMDARs, we first evaluated GluN2A surface levels in the dendrites of primary hippocampal neurons, by using a highly validated anti-GluN2A antibody recognizing the N-terminal domain[3,11]. We overexpressed mouse ortholog RFP-Rph3A^{WT}, RFP-Rph3A^{R206K} (corresponding to hRph3A^{R209K}), or RFP-Rph3A^{Q495H} (corresponding to hRph3A^{Q508H}) by transfection at *day in vitro* (*DIV) 8*, and endogenous GluN2A surface levels were analysed at *DIV16*, normalised to the intracellular subunit level. As shown in Fig. 1a-b, overexpression of both missense variants induced a significant increase in surface/intracellular ratio of GluN2A in dendrites compared with neurons overexpressing RFP-Rph3A^{WT} (RFP-Rph3A^{WT} vs. RFP-Rph3A^{R206K} *P Value = 0.0405; RFP-Rph3A^{WT} vs. RFP-Rph3A^{Q495H} *P Value = 0.0386), in absence of any significant modification of the intracellular levels (data not shown).

Depending upon subunit composition, NMDARs can be localised both at synaptic and extrasynaptic sites, and are highly mobile, diffusing laterally at the neuronal surface[14]. In physiological conditions, most surface NMDARs are located within the postsynaptic compartment, while only a small proportion are located extrasynaptically[15]. This is relevant, considering that the stimulation of extrasynaptic receptors can result in neurotoxicity and activation of intracellular cell death pathways[16]. Accordingly, we tested whether R206K and Q495H missense variants could alter NMDAR synaptic retention. To achieve this, we used the Airyscan super-resolution module for confocal microscopy to analyse the co-localisation of GluN2A with PSD-95, the main scaffolding protein of the excitatory post-synaptic density[2,17]. RFP-Rph3A^{WT}, RFP-Rph3A^{R206K}, or RFP-Rph3A^{Q495H} were overexpressed in hippocampal neurons at *DIV8* and an immunocytochemistry assay for GluN2A and PSD-95 was performed at *DIV16*. As shown in Fig. 1c-d, the percentage of GluN2A co-localizing with PSD-95 was decreased in neurons expressing both Rph3A missense variants compared to the WT protein (RFP-Rph3A^{WT} vs. RFP-Rph3A^{R206K} *P Value = 0.0438; RFP-Rph3A^{WT} vs. RFP-Rph3A^{Q495H} **P Value = 0.0054).

Rph3A missense variants do not affect NMDARs-dependent intracellular pathway

Considering these findings, which highlight an imbalance in NMDAR localisation between synaptic and extrasynaptic sites, we examined whether overexpression of either RFP-Rph3A^{R206K} and RFP-Rph3A^{Q495H} is sufficient to alter NMDAR-dependent downstream signalling events, such as the induction of CREB phosphorylation. In particular, it is well-demonstrated that the activation of synaptic NMDARs robustly promotes CREB phosphorylation at the activator-site residue Ser 133, thus inducing its nuclear translocation and activation of CREB-mediated gene expression[16]. In contrast, extrasynaptic NMDAR activation is associated with CREB shut-off pathways, promoting the expression of a set of genes distinct from those related to synaptic NMDARs. However, as indicated in Fig. 2a-b, we did not observe any significant changes in the level of pCREBSer133 in neurons expressing Rph3A missense variants compared to the WT protein. This suggests that Rph3A^{R206K} and Rph3A^{Q495H} variants do not affect this well-known NMDAR downstream signalling pathway.

Rph3A missense variants induce alteration of postsynaptic cytosolic calcium dynamics

The opening of postsynaptic NMDARs leads to calcium entry, which is responsible for the activation of downstream signalling cascades with important roles in synaptic activity and plasticity[18,19]. Having found altered GluN2A synaptic localisation in neurons overexpressing both Rph3A^{R206K} and Rph3A^{Q495H}, we investigated whether this was associated with altered postsynaptic calcium levels. To evaluate this possibility, neurons were transfected at *DIV8* with RFP-Rph3A^{WT}, RFP-Rph3A^{R206K}, or RFP-Rph3A^{Q495H}, along with the genetically encoded calcium indicator pCAG_Xph20-GCaMP7f, containing a moiety sensitive to PSD-95 to ensure enrichment of the indicator at dendritic spines (Fig. 3a). Accordingly, this approach allows for the precise evaluation of cytosolic calcium dynamics which are generated due to calcium influx through postsynaptic NMDARs. As shown in Fig. 3a-e and Supplementary Fig. 1, neurons overexpressing Rph3A^{R206K} or Rph3A^{Q495H} were characterised by altered postsynaptic calcium dynamics compared to Rph3A^{WT}. Aside from this, the analyses of the number of firing or silent spines in each condition demonstrated a decrease in the percentage of firing spines in neurons overexpressing Rph3A^{R206K} or Rph3A^{Q495H} (Fig. 3b). Meanwhile, we found that only the Rph3A^{Q495H} variant induced a significant decrease in the number of calcium events compared to neurons expressing the WT protein (Fig. 3d; RFP-Rph3A^{WT} vs. RFP-Rph3A^{Q495H} **P Value = 0.0046). Analysis of the area under the curve (AUC) did not show any changes resulting from the two Rph3A mutants compared to the WT protein (Fig. 3e).

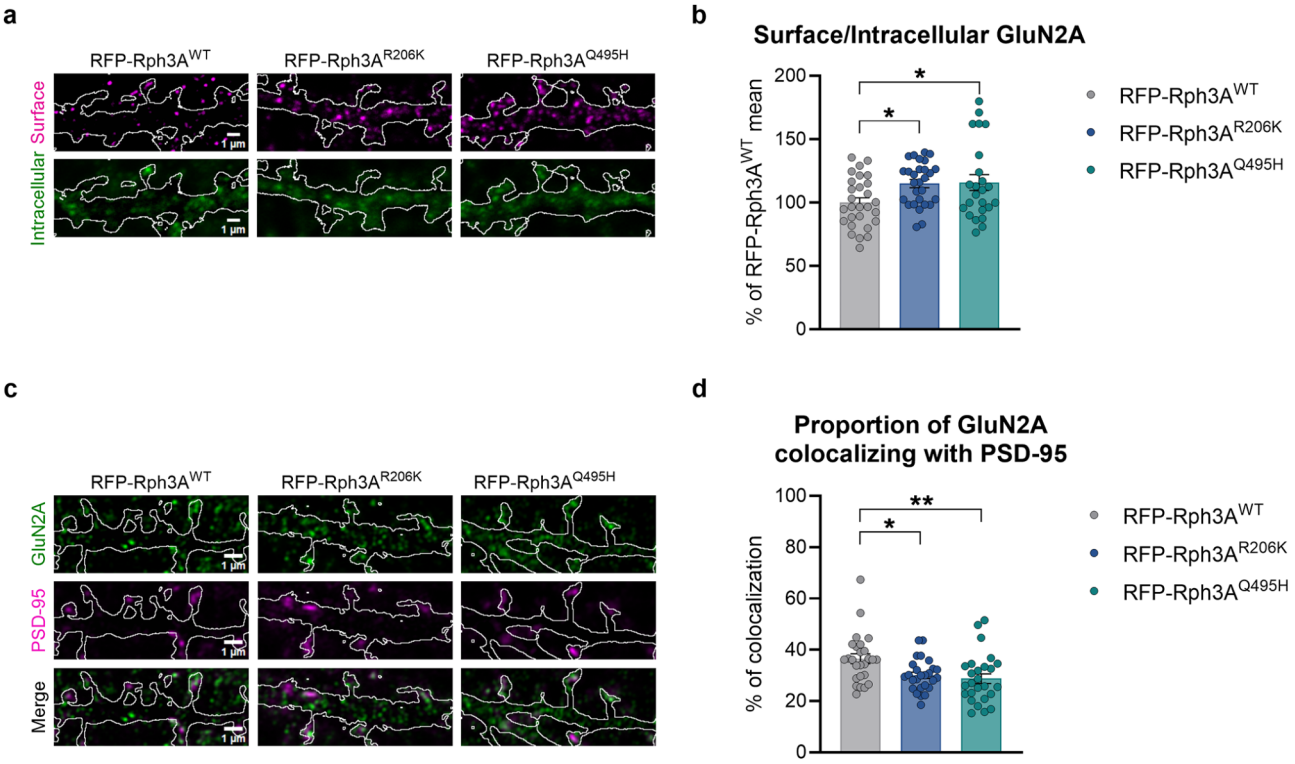

Fig. 1. *RPH3A* missense variants induce alterations of the surface and postsynaptic distribution of GluN2A-containing NMDARs. (**a**) Confocal images of surface (magenta) and intracellular GluN2A (green) staining in RFP-Rph3A^{WT}, RFP-Rph3A^{R206K}, or RFP-Rph3A^{Q495H} transfected neurons (outlined in white). Scale bar: 1 µm. (**b**) Bar graph representing the mean ± SEM of the percentage of RFP-Rph3A^{WT} mean GluN2A surface/intracellular ratio. Ordinary one-way ANOVA with Tukey's multiple comparisons post-hoc test (RFP-Rph3A^{WT} vs. RFP-Rph3AR^{206K} *P Value = 0.0405; RFP-Rph3A^{WT} vs. RFP-Rph3A^{Q495H} *P Value = 0.0386). The dots represent single values ($N = 28$ neurons, five independent experiments for RFP-Rph3A^{WT}; $N = 28$ neurons, five independent experiments for RFP-Rph3A^{R206K}; $N = 24$ neurons, five independent experiments for RFP-Rph3A^{Q495H}). (**c**) Airyscan confocal images of GluN2A (green) and PSD-95 (magenta) staining in RFP-Rph3A^{WT}, RFP-Rph3A^{R206K}, or RFP-Rph3A^{Q495H} transfected neurons (white outline). Scale bar: 1 µm. (**d**) Bar graph representing the mean ± SEM of the percentage of GluN2A colocalising with PSD-95. Kruskal-Wallis test with Dunn's post hoc test (RFP-Rph3A^{WT} vs. RFP-Rph3A^{R206K} *P Value = 0.0438; RFP-Rph3A^{WT} vs. RFP-Rph3A^{Q495H} **P Value = 0.0054). Dots represent single values ($N = 26$, five independent experiments for RFP-Rph3A^{WT}; $N = 26$, five independent experiments for RFP-Rph3A^{R206K}; $N = 26$, five independent experiments for RFP-Rph3A^{Q495H}).

Rph3A missense variants impair glutamatergic transmission

Rph3A was initially identified as a presynaptic Rab3A-binding protein[5], involved in the regulation of synaptic vesicle trafficking. To evaluate the possibility that Rph3A variants could affect both presynaptic and postsynaptic activity, we investigated their effects on glutamate release. Neurons were transfected at *DIV8* with either RFP-Rph3A^{WT}, RFP-Rph3A^{R206K}, or RFP-Rph3A^{Q495H} as well as with the postsynaptic glutamate-binding indicator, hSyn.iGluSnFR3.v857.SGZ. This indicator is targeted at the outer membrane via insertion between an N-terminal IgK secretion leader sequence and a C-terminal PDGFR transmembrane domain. In addition, this variant contains a PDGFR transmembrane domain, followed by a modified form of the cytosolic C-terminal domain of Stargazin (SGZ). This allows a better localisation of the glutamate sensor at the postsynaptic membrane[20]. The two Rph3A missense variants were both characterised by a significant alteration of glutamatergic transmission compared to Rph3A^{WT}, as shown in Fig. 4a-e and Supplementary Fig. 2. Specifically, the maximum intensity (Fig. 4b), number of glutamate events (Fig. 4c), and the AUC (Fig. 4d) were decreased significantly in both RFP-Rph3A^{R206K} and RFP-Rph3A^{Q495H} variants. These results suggest that mutations of Rph3A alter glutamate release, resulting in fewer glutamate events and lower levels of glutamate in the synaptic cleft.

Discussion

In recent years, numerous studies have highlighted the physiological role of Rph3A in excitatory glutamatergic synapses, mainly related to synaptic plasticity induction and its interaction with the NMDAR complex[1,3,4,21]. Notably, two independent analyses identified Rph3A as a key protein involved in cognitive resilience[22,23]. Additionally, recent research has linked Rph3A to both neurodevelopmental disorders[11] and neurodegenerative conditions, including Alzheimer's[22,24,25] and Parkinson's disease[26,27].

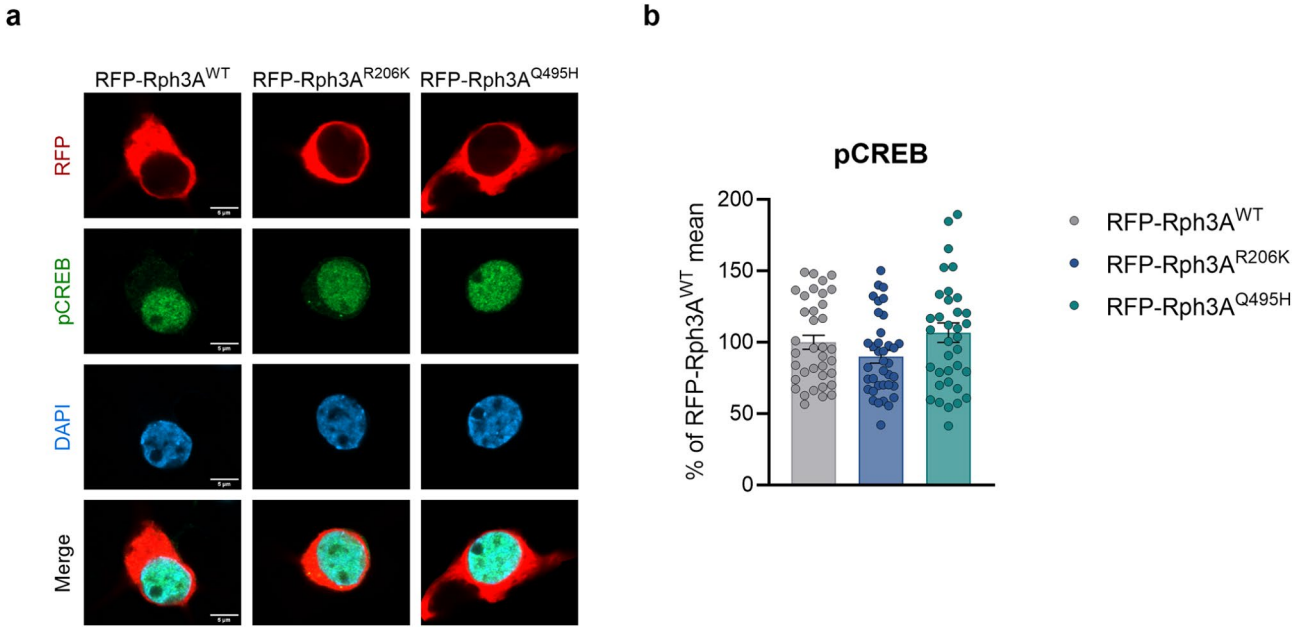

Fig. 2. *RPH3A* missense variants do not affect the NMDAR-dependent pCREB intracellular pathway. (**a**) Confocal images of pCREB (green) levels in RFP-Rph3A^{WT}, RFP-Rph3A^{R206K}, or RFP-Rph3A^{Q495H} transfected neurons (RFP signal in red). DAPI (blue) was used to stain the nuclei. Scale bar: 5 µm. (**b**) Bar graph representing the mean ± SEM of pCREB integrated density in the nucleus, expressed as the percentage of RFP-Rph3A^{WT} mean. Kruskal-Wallis test with Dunn's post-hoc test. The dots represent single values ($N = 36$ neurons, four independent experiments for RFP-Rph3A^{WT}; $N = 37$ neurons, four independent experiments for RFP-Rph3A^{R206K}; $N = 36$ neurons, four independent experiments for RFP-Rph3A^{Q495H}).

Our group recently reported six patients with missense variants in *RPH3A* who presented with either drug-resistant epilepsy with intellectual disability or as autism spectrum disorder with learning disability. We also characterised the molecular and functional impacts of two mutations, Rph3A^{T437S} and Rph3A^{N605S}, both located within the C-terminal C2 domains of the Rph3A protein. In this study, we extended these previous findings, demonstrating that two additional Rph3A variants, located at the N-terminal domain (Rph3A^{R206K}) or within the C-terminal domain (Rph3A^{Q495H}), induce significant but different effects on the NMDAR complex. Specifically, Rph3A^{Q495H} variant is located in the C2A domain, known to play key role for protein activity thanks to its role in the binding to Ca^{2+}/IP_3 binding[1]. Accordingly, similarly to what described for Rph3A^{T437S} variant, Rph3A^{Q495H} leads to a profound modifications of both GluN2A surface/synaptic localization and synaptic activity as indicated by alterations of postsynaptic calcium events. On the other hand, the Rph3A^{R206K} variant is located in the N-terminal disordered region of Rph3A, whose role is not well-described in the literature. Interestingly, this variant affects GluN2A surface/synaptic localization but does not influence the number of calcium events, thus suggesting a decreased synaptic phenotype associated to this N-terminal mutant.

Importantly, we provide also new insights into the effects of Rph3A variants on presynaptic glutamate release, showing that Rph3A mutants play a role in regulating excitatory synapse activity at both the pre- and post-synaptic compartments. Further identification of patients with genetic variants in *RPH3A* and neurodevelopmental disorders-related conditions will be fundamental to better understand eventual phenotype-genotype correlations.

Rph3A was initially identified as a putative target of Rab3a[5], a small G-protein involved in vesicle trafficking and neurotransmitter release. However, the role of Rph3A in the calcium-dependent neurotransmitter secretion pathway remains elusive and has not yet been fully characterised[28]. Interestingly, recent findings suggest that presynaptic Rph3A plays an important role in the storage and release of neuropeptides and neurotrophins through dense core vesicles[21]. In this study, we found that both the RFP-Rph3A^{R206K} and RFP-Rph3A^{Q495H} variants lead to a reduction in glutamate release events and lower glutamate levels in the synaptic cleft compared to Rph3A^{WT}. This suggests that Rph3A mutations not only affect postsynaptic activity but also presynaptic glutamate release, further confirming the wide-ranging roles of Rph3A at both sides of the glutamatergic synapse. Importantly, the decrease in glutamate release was accompanied by a reduction in the percentage of firing spines in neurons overexpressing Rph3A^{R206K} or Rph3A^{Q495H}; this aligns with our previous findings showing impaired postsynaptic calcium signalling in the dendritic spines of neurons transfected with Rph3A^{T437S} and Rph3A^{N605S}[11].

It can be hypothesised that the observed alterations in cytosolic calcium levels at dendritic spines may be associated with reduced glutamate release or modifications in postsynaptic NMDA receptors. We previously reported that overexpression of Rph3A^{WT} induces an increase of GluN2A colocalization with PSD-95[3]. Accordingly, the observed decrease of GluN2A/PSD-95 colocalization observed in neurons transected with Rph3A^{R206K} or Rph3A^{Q495H} compared to the WT protein suggest a *loss-of-function* phenotype of the two

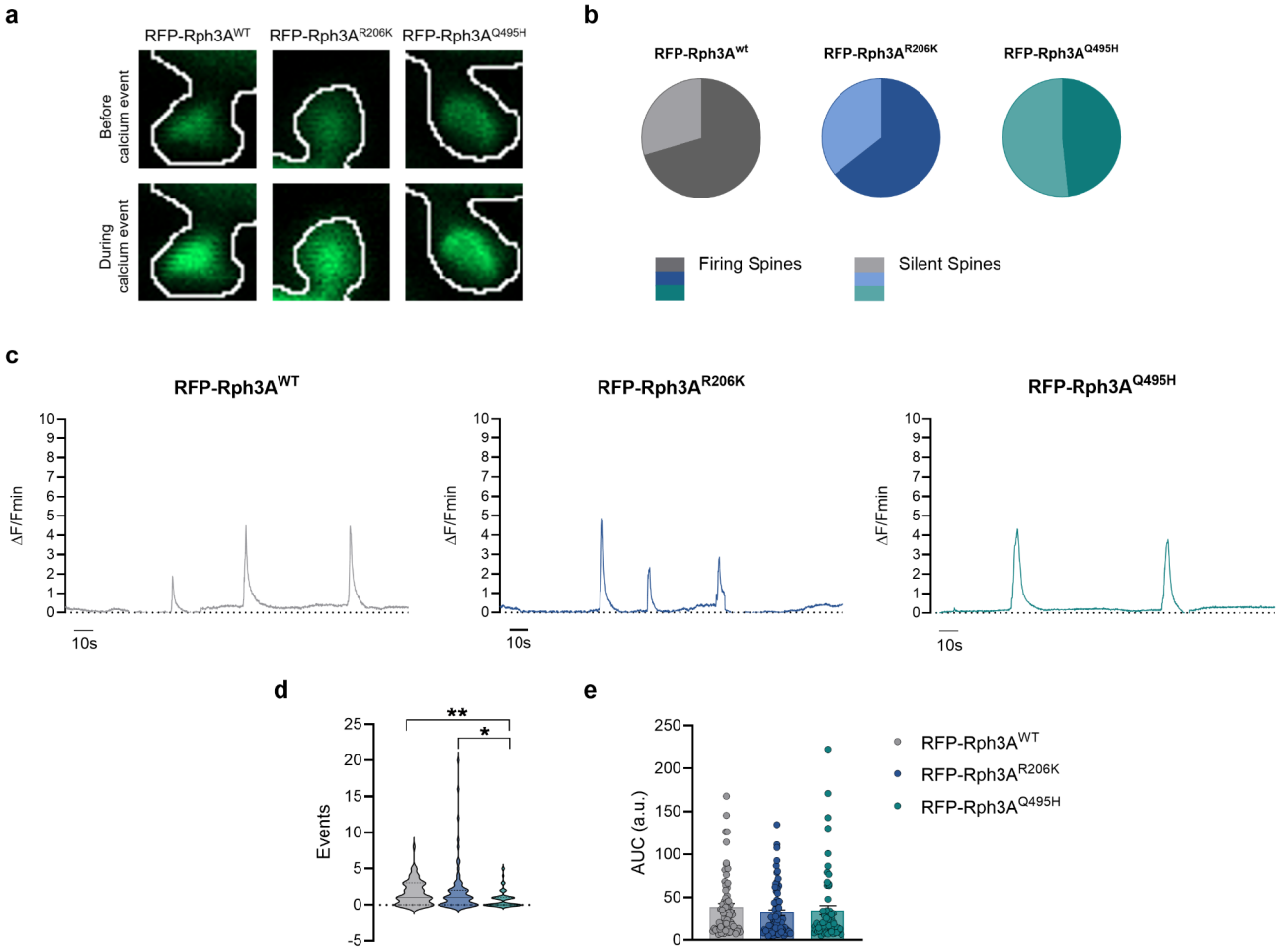

Fig. 3. *RPH3A* missense variants induce alteration of postsynaptic cytosolic calcium dynamics. (**a**) Confocal images of Xph20-GCaMP7f fluorescent signals before (upper images) and during (bottom images) a calcium event in a dendritic spine in RFP-Rph3A^{WT}, RFP-Rph3A^{R206K}, or RFP-Rph3A^{Q495H} transfected neurons. (**b**) Pie charts representing the percentage of firing spines in RFP-Rph3A^{WT} (70.42%), RFP-Rph3A^{R206K} (64.38%), and RFP-RpH3A^{Q495H} (48.33%) expressing neurons and the percentage of silent spines in RFP-Rph3A^{WT} (29.57%), RFP-Rph3A^{R206K} (35.61%), and RFP-RpH3A^{Q495H} (51.67%) expressing neurons. Firing spines are the ones experiencing 1 or more peaks (number of peaks > 0). (**c**) Representative Xph20-GCaMP7f fluorescent signal over time (3 min) in dendritic spines of *DIV16* primary hippocampal neurons transfected at *DIV8* with RFP-Rph3A^{WT}, RFP-Rph3A^{R206K}, or RFP-Rph3A^{Q495H} ($N = 71$ spines, five independent experiments for RFP-Rph3A^{WT}; $N = 73$ spines, five independent experiments for RFP-Rph3A^{R206K}; $N = 60$ spines, five independent experiments for RFP-Rph3A^{Q495H}). (**d**) Violin plot representing the number of events per spine over a 3-min period. Kruskal-Wallis' test with Dunn's post-hoc test (RFP-Rph3A^{WT} vs. RFP-Rph3A^{Q495H} **P Value = 0.0046; RFP-Rph3A^{R206K} vs. RFP-Rph3A^{Q495H} *P Value = 0.0433). Black lines represent the mean, and black dotted lines represent quartiles. (**e**) Bar graph representing the mean ± SEM of the area under the curve of spontaneous calcium transient events (evaluated as changes of Xph20-GCaMP7f fluorescence) at RFP-Rph3A^{WT}, RFP-Rph3A^{R206K}, and RFP-Rph3A^{Q495H} dendritic spine over 3 min. Kruskal-Wallis test with Dunn's post-hoc test.

mutants on GluN2A synaptic enrichment. This event also suggests an increase in the number of NMDARs at extrasynaptic sites. Consequently, the observed decrease in calcium events at dendritic spines associated with these two mutants may be explained by a reduced concentration of NMDARs at the postsynaptic membrane.

Finally, given these findings, which highlight imbalances in NMDAR localisation and activity between synaptic and extrasynaptic sites, we examined whether these changes are sufficient to alter NMDAR-dependent downstream signalling events, such as the induction of CREB phosphorylation[16]. However, we did not observe any significant alteration of CREB phosphorylation, suggesting that this well-known NMDAR downstream signalling pathway is not affected by Rph3A^{R206K} and Rph3A^{Q495H} variants.

In conclusion, our findings provide valuable information into the molecular mechanisms through which the *RPH3A* variants identified in patients lead to significant dysregulation of glutamatergic synaptic transmission. This work adds new insights to the understanding of the physiological and pathological roles of Rph3A in synaptic function.

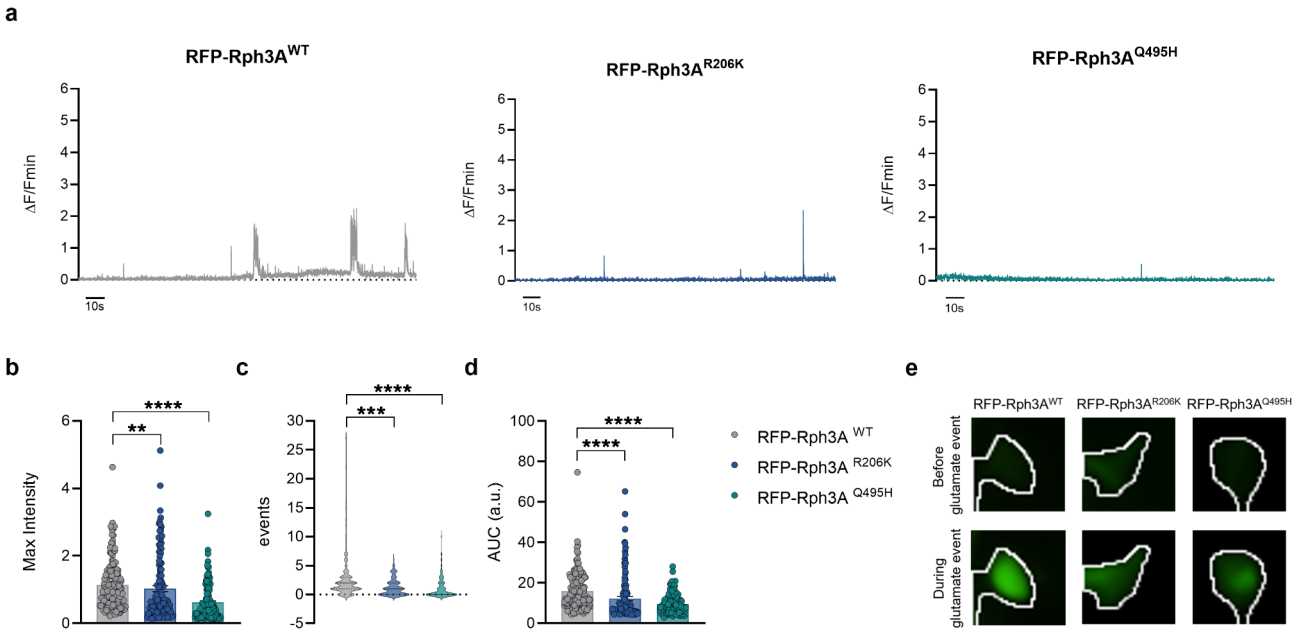

Fig. 4. *RPH3A* missense variants impair glutamatergic release. (**a**) Representative iGluSnFR3.sgz fluorescent signals over time (3 min) in *DIV16* primary hippocampal neurons transfected at *DIV8* with RFP-Rph3A^{WT}, RFP-Rph3A^{R206K}, or RFP-Rph3A^{Q495H} ($N = 152$ spines, five independent experiments for RFP-Rph3A^{WT}; $N = 119$ spines, five independent experiments for RFP-Rph3A^{R206K}; $N = 131$ spines, five independent experiments for RFP-Rph3A^{Q495H}). (**b**) Bar graph representing the mean ± SEM of the maximum intensity of glutamate events over a 3-min period. Kruskal-Wallis test with Dunn's post-hoc test (RFP-Rph3A^{WT} vs. RFP-Rph3A^{R206K} **P Value = 0.0017; RFP-Rph3A^{WT} vs. RFP-Rph3A^{Q495H} ****P Value < 0.0001). (**c**) Violin plot representing the number of glutamate events close to spines over a 3-min period. Kruskal-Wallis' test with Dunn's post-hoc test (RFP-Rph3A^{WT} vs. RFP-Rph3A^{R206K} ***P Value = 0.0002; RFP-Rph3A^{WT} vs. RFP-Rph3A^{Q495H} ****P Value < 0.0001). Black lines represent the mean, and black dotted lines represent quartiles. (**d**) Bar graph representing the mean ± SEM of the area under the curve of glutamate transient events (evaluated as changes of iGluSnFR3.sgz fluorescence) at RFP-Rph3A^{WT}, RFP-Rph3A^{R206K}, and RFP-Rph3A^{Q495H} dendritic spines over 3 min. Kruskal-Wallis test with Dunn's post-hoc test (RFP-Rph3A^{WT} vs. RFP-Rph3A^{R206K} ****P Value < 0.0001; RFP-Rph3A^{WT} vs. RFP-Rph3A^{Q495H} ****P Value < 0.0001). (**e**) Confocal images of iGluSnFR3.sgz fluorescent signals before (upper images) and during (bottom images) a glutamate event in a dendritic spine in RFP-Rph3A^{WT}, RFP-Rph3A^{R206K}, or RFP-Rph3A^{Q495H} transfected neurons.

Materials and methods

Primary hippocampal neuronal cultures

Hippocampal primary neuronal cultures were prepared from embryonic day 18–19 (E18–E19) Sprague-Dawley rat hippocampi (Charles River Laboratories, Calco, Italy). All procedures involving animals were reported in accordance with ARRIVE guidelines, were approved by the Italian Ministry of Health and the local Animal Use Committee (project n°: 5247B.N.YOX) and were conducted according to the Guide for the Care and Use of Laboratory Animals of the National Institutes of Health and the European Community Council Directives. On the 18th -19th gestational day, the pregnant rats were anesthetized by inhalation of isoflurane (5%). After verifying the effectiveness of the anesthesia (immobility of the animal and absence of voluntary and involuntary movements), the rats were immediately sacrificed by decapitation. Hippocampi were rapidly dissected by embryos under sterile conditions, kept in cold Hanks' balanced saline solution (4 °C) with high glucose, and then digested with trypsin (Gibco). Isolated cells were plated at a final density of 75 000 cells/mm^2 on ⌀14 mm diameter coverslips in a 12-well plate coated with poly-L-lysine (1 mg/mL, Sigma-Aldrich) dissolved in borate buffer overnight for immunocytochemistry, or 250 000 cells/mm^2 on ⌀14 mm glass diameter or in a ⌀35 mm dish (MatTek) coated with poly-L-lysine (1 mg/mL, Sigma-Aldrich) dissolved in borate buffer overnight for live imaging experiments. Neurons were plated in plating medium consisting of DMEM + Glutamax (Gibco), completed with 10% horse serum (Gibco), 1% penicillin, and streptomycin (pen/strep, Euroclone). The medium was replaced with Neurobasal medium (NB, Gibco), supplemented with 2% B27 (Gibco), 1% pen/strep, and 1% Glutamax (Gibco) the following day, and kept in 5% CO_2 at 37 °C.

Transfection and plasmids

Cells were transfected on *DIV8* using the calcium-phosphate method. For live imaging, for each MatTek, a total of 6 µg of DNA was added (3 µg of pCAG_Xph20-GCaMP7f or pAAV.hSyn.iGluSnFR3.v857.SGZ + 3 µg of AAV9-hSyn-RFP-Rph3A-WPRE, hSyn-RFP-Rph3AR206K-WPRE or hSyn-RFP-Rph3AQ495H-WPRE). Neurobasal medium was collected and replaced with Minimum Essential Medium (MEM) + Glutamax (Gibco)

an hour before transfection. DNA precipitates were prepared with 6 µg of DNA and 12.5 µL of 2.5 M $CaCl_2$ and brought to a final volume of 100 µL with dH_2O. This solution was mixed with 100 µL of HBS 2x and left to incubate for 30 min at room temperature (RT). These DNA precipitates were added to the MatTek in a dropwise manner. After 10–15 min of incubation, neurons were washed with MEM + Glutamax and the medium was replaced with the old NB medium topped up with new NB complete medium, to reach a final volume of 3 mL of medium per MatTek. For immunostaining, transfection was performed as previously reported, but a total of 2 µg of DNA was added per well (AAV9-hSyn-RFP-Rph3A-WPRE, hSyn-RFP-Rph3AR206K-WPRE, or hSyn-RFP-Rph3AQ495H-WPRE). DNA precipitates were prepared with 4 µg of DNA and 10 µL of 2.5 M $CaCl_2$, and brought to a final volume of 80 µL with dH_2O. This solution was mixed with 80 µL of HBS 2x and left to incubate for 30 min at RT. Eighty µL of DNA precipitates were added into one well in a dropwise manner. After 10–15 min of incubation, neurons were washed with MEM + Glutamax and the medium was replaced with the old NB medium topped up with new NB medium to reach a final volume of 1mL of medium per well.

The AAV9-hSyn-RFP-Rph3A-WPRE plasmids were purchased from Addgene. The hSyn-RFP-Rph3AR206K-WPRE and hSyn-RFP-Rph3AQ495H-WPRE were produced and purchased from Vector Builder. pCAG_Xph20-GCaMP7f was a gift from Matthieu Sainlos (Addgene plasmid #135539; http://n2t.net/addgene:135539; RRID: Addgene_135539). pAAV.hSyn.iGluSnFR3.v857.SGZ was a gift from Kaspar Podgorski (Addgene plasmid #178330; http://n2t.net/addgene:178330; RRID).

Immunocytochemistry

For colocalisation studies and pCREB experiments, transfected hippocampal neurons at *DIV16* were fixed for 10 min at RT in 4% paraformaldehyde and 4% sucrose in Dulbecco's phosphate-buffered saline (PBS). Coverslips were then washed with PBS, permeabilised with 0.1% Triton X-100 in PBS for 15 min at RT, and blocked for 30 min at RT with 5% bovine serum albumin (BSA) in PBS. Cells were then incubated with primary antibodies in 5% BSA-PBS overnight at 4 °C in a humidified chamber. After washing with PBS, the cells were incubated with the fluorophore-conjugated secondary antibodies in 5% BSA-PBS for 1 h at RT in a humidified chamber protected from light. The incubation was followed by washing with PBS and mounting onto glass slides using Fluoroshield mounting medium (Sigma-Aldrich). For pCREB experiments, cells were incubated with the nuclear stain DAPI before mounting onto glass slides.

Surface staining assays were performed as previously reported with certain modifications[1,3,11]. Transfected hippocampal neurons were fixed at *DIV16* for 10 min at RT in 4% paraformaldehyde and 4% sucrose in Dulbecco's PBS. Coverslips were washed with PBS and then blocked for 30 min at RT with 5% BSA in PBS. Cells were not permeabilised, and were labelled for 1 h at RT with primary antibodies (anti-GluN2A) recognising an extracellular epitope at the N-terminal region of the subunits. This procedure allows for surface staining by targeting the epitope in the extracellular domain. The coverslips were then washed in PBS and a secondary antibody conjugated to Alexa Fluor dye was used. The coverslips were then washed with PBS, permeabilised with 0.1% Triton X-100 in PBS for 15 min, and blocked for 30 min at RT with 5% BSA in PBS. Cells were then incubated with the same primary antibodies in 5% BSA-PBS for 1 h at 4 °C in a humidified chamber to detect the intracellular subunit. After washes with PBS, the cells were incubated with the fluorophore-conjugated secondary antibodies in 5% BSA-PBS for 1 h in a humidified chamber protected from light. The incubation was followed by washing with PBS and mounting onto glass slides using Fluoroshield mounting medium (Sigma-Aldrich). Cells from different coverslips from independent experiments were randomly chosen for quantification and images were acquired using LSM900 (Zeiss) confocal microscopes with a 63× NA1.42 objective at a 0.09 µm pixel size. For super-resolution assays, images were taken using the Airyscan mode on an LSM900 confocal microscope (Zeiss) with a 63× NA1.42 objective at a 0.04 mm pixel size.

For all imaging experiments, neuronal transfection of Rph3A constructs was always evaluated by the presence of the RFP red signal. During acquisition with LSM900 confocal microscope, images were taken with the application of "range indicator", a specific tool that allows visualizing the level of saturation. All the images were taken below the saturation level. For the quantification of surface/intracellular staining of GluN2A, analysis were conducted with ImageJ software. After selecting as a "region of interest" (ROI) the transfected neuron, evaluated by the presence of RFP red signal, the mean value of the fluorescence intensity of pixel inside the ROI was measured for both surface GluN2A and intracellular GluN2A. Then, the ratio between the mean value of surface GluN2A and intracellular GluN2A was calculated.

For pCREB experiments, we evaluated its fluorescence specifically at the nuclear level. Nuclei were identified using the nuclear stain DAPI and a ROI has been created on it. pCREB fluorescence was measured, evaluating the integrated density of fluorescence signal of pCREB inside the ROI. All values were then normalized to the mean pCREB fluorescence of the control group.

Analysis of GCaMP7 fluorescent signals

Calcium imaging experiments using the pCAG_Xph20-GCaMP7f calcium indicator were performed in primary hippocampal neuronal cultures at *DIV16*. Live-cell imaging acquisition was performed using an LSM900 (Zeiss) confocal microscope with a 63× NA1.42 objective. Dendrites were imaged at maximum scanning speed with a 6.7 zoom (scan time around 35 ms, resolution: 0.07 nm/pixel). Time-lapse images were taken for 3 min at 10 Hz. NB medium was replaced with artificial cerebral spinal fluid (ACSF: 125 mM $NaCl_2$, 2.5 mM KCl, 1 mM $MgCl_2$, 33 mM Glucose, 25 mM HEPES, 2 mM $CaCl_2$, and dH_2O; pH: 7.4–7.5) and neurons were kept at 37 °C with 5% CO_2 throughout the imaging procedure. After recording the GCaMP7f's signal in live imaging, we applied selective NMDAR antagonist 2-amino-5-phosphonovaleric acid (APV) at a final concentration of 50 µM in the medium and then immediately recorded the fluorescent signal at the same position. GCaMP7f's transients were almost fully abolished (>95%) by administering APV (data not shown), indicating that the postsynaptic Ca^{2+} currents detected under our experimental conditions depended on NMDAR activation.

For quantitative analysis, dendritic spines were chosen as regions of interest, and GCaMP7f fluorescence was plotted over time using ImageJ. For each region of interest, we computed the number of every cytosolic calcium transient event showing a $\Delta F/F_{min}$ over 0.5 in a time window of 3 min, and the area under the $\Delta F/F_{min}$ curve, with Fmin being the baseline value of fluorescent intensity. Spines without any transients over the 3-minute period were categorised as silent, whereas those exhibiting at least one transient were classified as firing.

Analysis of iGluSnFR3.sgz fluorescent signals

Glutamate imaging experiments using pAAV.hSyn.iGluSnFR3.v857.SGZ were performed in primary hippocampal neuronal cultures at *DIV16*. Live-cell imaging was performed using a Nikon Eclipse Ti2 inverted confocal microscope with a CFI Apochromat TIRF 60x/1.49XC oil objective, with a 4x zoom (scan time of 21.2 ms and a resolution of 0.2 µm/pixel). Time-lapse images were taken for 3 min at 20 Hz. NB medium was replaced with ACSF (125 mM $NaCl_2$, 2.5 mM KCl, 1 mM $MgCl_2$, 33 mM Glucose, 25 mM HEPES, 2 mM $CaCl_2$, and dH_2O; pH: 7.4–7.5) and neurons were kept at 37 °C with 5% CO_2 throughout the imaging procedure. For quantitative analysis, dendritic spines were chosen as regions of interest, and the iGluSnFR3.sgz fluorescence was plotted over time using ImageJ. For each region of interest, we computed the number of every glutamate transient event showing a $\Delta F/F_{min}$ over 0.5 in a time window of 3 min, and the area under the $\Delta F/F_{min}$ curve, with Fmin being the baseline value of fluorescent intensity.

Antibodies

The following primary antibodies were used: rabbit anti-N-term-GluN2A (480031, Invitrogen; dilution 1:100 ICC), mouse anti-RFP (OAEA00012, Aviva; dilution 1:500 ICC), mouse anti-PSD-95 (192757, Abcam; dilution 1:1000 ICC), rabbit anti-p-CREB Ser-133 (06-519 Millipore, dilution 1:250 ICC), and DAPI.

The following secondary antibodies were used: goat anti-rabbit-AlexaFluor488 (A21206, Life Technologies; dilution 1:1000 ICC), goat anti-rabbit-AlexaFluor647 (A21245, Life Technologies; dilution 1:1000 ICC), goat anti-mouse-AlexaFluor647 (A21235, Invitrogen; dilution 1:1000), and goat anti-mouse-AlexaFluor555 (A-21424, Invitrogen; dilution 1:1000 ICC).

Data presentation and statistical analysis

All group values are expressed as mean ± SEM. Normality was evaluated using D'Agostino-Pearson or Shapiro-Wilk tests. Comparisons between groups were performed using the following tests, as appropriate: two-tailed unpaired Student's t-test, Mann-Whitney U test, one-way analysis of variance (ANOVA) followed by post-hoc tests. Outliers were identified with the ROUT method (Q = 5%). Significance was defined as $p < 0.05$. All statistical analyses were performed using the GraphPad Prism statistical package (GraphPad software). Sample sizes for the specific types of experiments conducted were determined based on those generally employed in the field. Immunocytochemical and live imaging experiments were acquired at confocal microscope and quantified under blind conditions.

Ethics declaration

As previously reported[11], informed consent was obtained from participating families, and the study protocol was approved by the Internal Ethics Committee of the University of Turin (n. 0060884), in accordance to the Declaration of Helsinki. Part of the cases were collected within the 100,000 Genomes Project and had specific ethical approval. All experiments were performed in accordance with relevant guidelines and regulations.

Data availability

The datasets analyzed during the current study are available from the corresponding author on reasonable request.

Received: 21 November 2024; Accepted: 6 March 2025
Published online: 13 March 2025

References

1. Stanic, J. et al. Rabphilin 3A retains NMDA receptors at synaptic sites through interaction with GluN2A/PSD-95 complex. *Nat. Commun.* **6**, 10181 (2015).
2. Franchini, L. et al. Linking NMDA receptor synaptic retention to synaptic plasticity and cognition. *Iscience* **19**, 927–939 (2019).
3. Franchini, L. et al. Rabphilin-3A drives structural modifications of dendritic spines induced by long-term potentiation. *Cells* **11** (10), 1616 (2022).
4. Yang, L. et al. Rabphilin-3A undergoes phase separation to regulate GluN2A mobility and surface clustering. *Nat. Commun.* **24**, 379 (2024).
5. Burns, M. E., Sasaki, T., Takai, Y. & Augustine, G. J. Rabphilin-3A: a multifunctional regulator of synaptic vesicle traffic. *J. Gen. Physiol.* **111**, 243–255 (1998).
6. Zhang, Y., Luan, Z., Liu, A. & Hu, G. The scaffolding protein CASK mediates the interaction between rabphilin3a and beta-neurexins. *FEBS Lett.* **497**, 99–102 (2001).
7. Guillén, J. et al. Structural insights into the Ca2 + and PI(4,5)P2 binding modes of the C2 domains of rabphilin3A and synaptotagmin 1. *Proc. Natl. Acad. Sci. USA.* **110**, 20503–20508 (2013).
8. Ferrer-Orta, C. et al. Structural characterization of the Rabphilin-3A-SNAP25 interaction. *Proc. Natl. Acad. Sci. USA.* **114**, E5343–E5351 (2017).
9. Ren, C. et al. Small GTPase ARF6 is a coincidence-detection code for RPH3A polarization in neutrophil polarization. *J. Immunol.* **204**, 1012–1021 (2020).
10. Brozzi, F. et al. Molecular mechanism of myosin Va recruitment to dense core secretory granules. *Traffic* **13**, 54–69 (2012).
11. Pavinato, L. et al. Missense variants in RPH3A cause defects in excitatory synaptic function and are associated with a clinically variable neurodevelopmental disorder. *Genet. Med.* **25**, 100922 (2023).

12. Maselli, R. A. et al. Presynaptic congenital myasthenic syndrome with altered synaptic vesicle homeostasis linked to compound heterozygous sequence variants in RPH3A. *Mol. Genet. Genomic Med.* **6**, 434–440 (2018).
13. Montaville, P. et al. The C2A-C2B linker defines the high affinity Ca(2+) binding mode of rabphilin-3A. *J. Biol. Chem.* **282**, 5015–5025 (2007).
14. Groc, L. et al. Differential activity-dependent regulation of the lateral mobilities of AMPA and NMDA receptors. *Nat. Neurosci.* **7**, 695–696 (2004).
15. Harris, A. Z. & Pettit, D. L. Extrasynaptic and synaptic NMDA receptors form stable and uniform pools in rat hippocampal slices. *J. Physiol.* **584**, 509–519 (2007).
16. Hardingham, G. E. & Bading, H. Synaptic versus extrasynaptic NMDA receptor signalling: implications for neurodegenerative disorders. *Nat. Rev. Neurosci.* **11**, 682–696 (2010).
17. Paoletti, P., Bellone, C. & Zhou, Q. NMDA receptor subunit diversity: impact on receptor properties, synaptic plasticity and disease. *Nat. Rev. Neurosci.* **14**, 383–400 (2013).
18. Malenka, R. C. The role of postsynaptic calcium in the induction of long-term potentiation. *Mol. Neurobiol.* **5**, 289–295 (1991).
19. Malenka, R. C. & Nicoll, R. A. NMDA-receptor-dependent synaptic plasticity: multiple forms and mechanisms. *Trends Neurosci.* **16** (12), 521–527 (1993).
20. Aggarwal, A. et al. Glutamate indicators with improved activation kinetics and localization for imaging synaptic transmission. *Nat. Methods*. **20** (6), 925–934 (2023).
21. Abramian, A. et al. Rabphilin-3A negatively regulates neuropeptide release, through its SNAP25 interaction. *Elife* **13**, RP95371 (2024).
22. Yu, L. et al. Cortical proteins associated with cognitive resilience in community-dwelling older persons. *JAMA Psychiatry*. **1**, 1172–1180 (2020).
23. Poole, V. N. et al. Associations of brain morphology with cortical proteins of cognitive resilience. *Neurobiol. Aging*. **137**, 1–7 (2024).
24. Tan, M. G. et al. Decreased rabphilin 3A immunoreactivity in Alzheimer's disease is associated with Abeta burden. *Neurochem Int.* **64**, 29–36 (2014).
25. Nguyen, D. P. Q. et al. Multiple transcriptomic analyses explore potential synaptic biomarker rabphilin-3A for Alzheimer's disease. *Sci. Rep.* **14**, 18717 (2024).
26. Ferrari, E. et al. Rabphilin-3A as a novel target to reverse alpha-synuclein-induced synaptic loss in Parkinson's disease. *Pharmacol. Res.* **183**, 106375 (2022).
27. Sawant, R. & Godad, A. An update on novel and emerging therapeutic targets in Parkinson's disease. *Metab. Brain Dis.* **39**, 1213–1225 (2024).
28. Bourgeois-Jaarsma, Q., Miaja Hernandez, P. & Groffen, A. J. Ca2 + sensor proteins in spontaneous release and synaptic plasticity: limited contribution of Doc2c, rabphilin-3a and synaptotagmin 7 in hippocampal glutamatergic neurons. *Mol. Cell. Neurosci.* **112**, 103613 (2021).

Acknowledgements

This work was supported by grant from MUR Progetto Eccellenza (2023-2027) to the Department of Pharmacological and Biomolecular Sciences "Rodolfo Paoletti"; PRIN Bando 2022, Prot. 2022YY85P5 to FG; PNRR, Missione 4 – Componente 2– Investimento 1.3, finanziato dall'Unione europea – NextGenerationEU "Fascination" to M.D. and FIS00000560 – "Stone" to M.D. The authors thank Chiara Galizia for her excellent practical work. Part of this work was conducted at NOLIMITS, an advanced imaging facility established by the University of Milan.

Author contributions

M.B.: writing – original draft, investigation, data curation. A.S.: investigation, data curation. Alex Costa: methodology, writing – review & editing. L.P.: investigation, conceptualization, writing – review & editing. A.B.: conceptualization, resources, writing – review & editing. E.M.: formal analysis, writing – review & editing. M.D.: conceptualization, funding acquisition, supervision, writing – review & editing. F.G.: writing – original draft, funding acquisition, data curation, conceptualization.

Declarations

Competing interests

The authors declare no competing interests.

Additional information

Supplementary Information The online version contains supplementary material available at https://doi.org/10.1038/s41598-025-93403-9.

Correspondence and requests for materials should be addressed to F.G.